Physica A 409 (2014) 35–47

Contents lists available at ScienceDirect

Physica A

journal homepage: www.elsevier.com/locate/physa

Toward a theory of topopatric speciation: The role of genetic assortative mating

David M. Schneider [a,*], Eduardo do Carmo [b], Ayana B. Martins [c], Marcus A.M. de Aguiar [a]

[a] Instituto de Física 'Gleb Wataghin', Universidade Estadual de Campinas, Unicamp, 13083-859, Campinas, SP, Brazil
[b] Universidade Federal da Integração Latino Americana, 85867-970, Foz do Iguaçu, PR, Brazil
[c] Instituto de Biociências, Universidade de São Paulo, 05508-090, São Paulo, SP, Brazil

HIGHLIGHTS

- We derive the equations for the haplotype frequencies under assortative mating.
- We find equilibrium solutions and study their stability.
- Equilibria are characterized by the disappearing of one allele.
- We study times of convergence to equilibria.
- Certain combination of allele frequencies remains constant throughout the dynamics.

ARTICLE INFO

Article history:
Received 23 December 2013
Received in revised form 11 March 2014
Available online 1 May 2014

Keywords:
Models of speciation
Assortative mating
Population genetics
Haplotype frequency
Fixed point stability
Constant of motion

ABSTRACT

We discuss a minimalist model of assortative mating for sexually reproducing haploid individuals with two biallelic loci. Assortativeness is introduced in the model by preventing mating between individuals whose alleles differ at both loci. Using methods of dynamical systems and population genetics we provide a full description of the evolution of the system for the case of very large populations. We derive the equations governing the evolution of haplotype frequencies and study the equilibrium solutions, stability, and speed of convergence to equilibrium. We find a constant of motion which allows us to introduce a geometrical construction that makes it straightforward to predict the fate of initial conditions. Finally, we discuss the consequences of this class of assortative mating models, including their possible extensions and implications for sympatric and topopatric speciation.

1. Introduction

While the origin of species has always been a central subject in evolutionary biology, the large number of recent empirical and theoretical developments has renewed the interest in the area [1–4]. Among the vast body of literature, individual-based simulations have shown to be specially important in fostering relevant discussions in speciation [5–17]. Within this class we find a neutral model of speciation formulated by de Aguiar and coworkers, which successfully predicts empirical patterns of species diversity [13]. Simulations of the model demonstrate that even in the absence of natural selection speciation can

* Corresponding author. Tel.: +55 19 3521 5463.
E-mail address: schneide@ifi.unicamp.br (D.M. Schneider).

http://dx.doi.org/10.1016/j.physa.2014.04.026
0378-4371/

occur as a consequence of two reinforcing trends: isolation mediated by spatial distance and isolation mediated by genetic incompatibility. Originally studied by Sewall Wright in 1943 [18], isolation by spatial distance involves a physical mating restriction modeled through a parameter S, representing the search radius for the individuals to find a potential partner. Isolation by genetic incompatibility, on the other hand, is included in the model by preventing mating between individuals whose genetic distance (defined as the number of loci displaying different alleles) exceeds a maximum tolerable difference of G. The latter scheme of assortativeness was introduced by Higgs and Derrida [5], and is motivated by the fact that mate choice often relies on multiple cues that are determined genetically [19].

As speciation in this context occurs in a single non-panmictic population, the model could be considered parapatric [20]. However, the geographical context of speciation is usually defined in terms of the ranges of the initial populations or the amount of gene flow between different demes. In this case, populations are said to be parapatric when the initial allelic exchange rate is neither zero nor maximum [2]. Even though this definition of parapatry is very broad and turns sympatry and allopatry into limiting cases, it still does not describe precisely the scenario adopted by the model of Aguiar and coworkers. Since individuals have to be sufficiently close to each other in space to reproduce, there is an explicit mechanism acting on the individuals that leads to a spatially structured population and isolation by distance. There are no predefined population ranges: ranges develop spontaneously during the evolution of an initially uniformly distributed population. It resembles a ferromagnetic phase transition, in the course of which a symmetry is broken leading to the formation of quasi-homogeneous clusters [21]. In the present framework, the clusters correspond precisely to species. Therefore, to emphasize the spatial mechanism that does not rely on assumptions about the range of the nascent species the term topopatry was adopted.

In this paper we give a first step in the construction of a population genetics theory for topopatric speciation by considering the simplest example in which the effect of assortative mating may be implemented. Specifically, we analyze the dynamics of a population of haploid and hermaphrodite individuals bearing only two biallelic loci. We further assume that sexual reproduction is possible between individuals whose haplotypes differ in at most one locus, i.e., the maximum allowed genetic distance is $G = 1$. We perform a detailed examination of the dynamics of haplotype and allele frequencies for the case of an infinitely large population with no mutations.

The paper is organized as follows: in Section 2 we describe a general reproductive mechanism that allows for the construction of different mating models, including assortativeness based on genetic compatibility. In Section 3 we briefly consider the case of random mating. Evolution under assortative mating is analyzed in Section 4, including the description of equilibria and their stability, rates of convergence, and constants of motion. Finally, in Section 5 we expose our conclusions and discuss the possible consequences of our results for the sympatric and topopatric speciations. Auxiliary mathematical material is included in appendices.

2. Reproductive model

Consider a population of hermaphrodite individuals with haploid genomes consisting of two biallelic loci. The state of the population in the generation t can be specified by the number of individuals having each of the four possible haplotypes, AB, Ab, aB, and ab, where A and a are the alleles at one locus, and B and b the alleles at the other. These numbers are denoted by N^t_{AB}, N^t_{Ab}, N^t_{aB} and N^t_{ab}, with $N^t_{AB} + N^t_{Ab} + N^t_{aB} + N^t_{ab} = N^t$, the total size of the population. Encounters between the members of this generation may succeed or not in producing offspring for the generation $t + 1$, depending on the probabilities $w_{h_1:h_2}$ (h_1 and h_2 being the parental haplotypes). The rates $w_{h_1:h_2}$ (see Table 1) incorporate both the effects of the compatibility between the parents (sexual selection) and the viability of the newly formed zygote (viability selection). In our model the viability selection is the same for all individuals, and takes place once the zygote was formed through the inheritance of a recombinated chromosome (the recombination of the parental chromosomes occurs at a recombination rate r). Assortativeness, represented by the sexual selection component, is described by the compatibility between the parents and acts at a prezygotic level. The reason for adding a postzygotic factor to the compound fitness $w_{h_1:h_2}$, from now on the compatibility–viability selection rate, has the only purpose of keeping the total number of individuals constant across generations, and represents an implicit carrying capacity, i.e., finite abundance of resources.

According to Table 1, and assuming non-overlapping generations, the number of AB individuals in the generation $t + 1$ obeys

$$\begin{aligned} N^{t+1}_{AB} = {} & \frac{1}{2}N^t_{AB}(N^t_{AB} - 1)w_{AB:AB} + \frac{1}{2}N^t_{AB}N^t_{Ab}w_{AB:Ab} + \frac{1}{2}N^t_{AB}N^t_{aB}w_{AB:aB} \\ & + \frac{r}{2}N^t_{AB}N^t_{ab}w_{AB:ab} + \frac{1-r}{2}N^t_{Ab}N^t_{aB}w_{Ab:aB}. \end{aligned} \tag{1}$$

The evolution equations for the other haplotypes can be obtained similarly:

$$\begin{aligned} N^{t+1}_{Ab} = {} & \frac{1}{2}N^t_{Ab}(N^t_{Ab} - 1)w_{Ab:Ab} + \frac{1}{2}N^t_{AB}N^t_{Ab}w_{AB:Ab} + \frac{1}{2}N^t_{Ab}N^t_{ab}w_{Ab:ab} \\ & + \frac{r}{2}N^t_{AB}N^t_{ab}w_{AB:ab} + \frac{1-r}{2}N^t_{Ab}N^t_{aB}w_{Ab:aB} \end{aligned} \tag{2}$$

Table 1
Encounters between individuals in the generation t that contribute to individuals with haplotype AB in the generation $t+1$.

Paternal haplotypes	Number of encounters	Fraction of successful AB offspring
$AB \times AB$	$\frac{1}{2}N^t_{AB} \times (N^t_{AB}-1)$	$w_{AB:AB}$
$AB \times Ab$	$N^t_{AB} \times N^t_{Ab}$	$1/2 \times w_{AB:Ab}$
$AB \times aB$	$N^t_{AB} \times N^t_{aB}$	$1/2 \times w_{AB:aB}$
$AB \times ab$	$N^t_{AB} \times N^t_{ab}$	$(1-r)/2 \times w_{AB:ab}$
$Ab \times aB$	$N^t_{Ab} \times N^t_{aB}$	$r/2 \times w_{Ab:aB}$

$$N^{t+1}_{aB} = \frac{1}{2}N^t_{aB}(N^t_{aB}-1)w_{aB:aB} + \frac{1}{2}N^t_{AB}N^t_{aB}w_{AB:aB} + \frac{r}{2}N^t_{aB}N^t_{ab}w_{aB:ab} + \frac{r}{2}N^t_{AB}N^t_{ab}w_{AB:ab} + \frac{1-r}{2}N^t_{Ab}N^t_{aB}w_{Ab:aB} \tag{3}$$

$$N^{t+1}_{ab} = \frac{1}{2}N^t_{ab}(N^t_{ab}-1)w_{ab:ab} + \frac{1}{2}N^t_{Ab}N^t_{ab}w_{Ab:ab} + \frac{1}{2}N^t_{aB}N^t_{ab}w_{aB:ab} + \frac{r}{2}N^t_{AB}N^t_{ab}w_{AB:ab} + \frac{1-r}{2}N^t_{Ab}N^t_{aB}w_{Ab:aB}. \tag{4}$$

In the following sections we analyze, in the limit of very large populations, the dynamics of the haplotype frequencies

$$p^t_{AB} = N^t_{AB}/N^t \tag{5}$$
$$p^t_{Ab} = N^t_{Ab}/N^t \tag{6}$$
$$p^t_{aB} = N^t_{aB}/N^t \tag{7}$$
$$p^t_{ab} = N^t_{ab}/N^t. \tag{8}$$

For each different scenario we specify the values of the compatibility–viability selection rates by imposing the corresponding (prezygotic) mating scheme and setting the total number of individuals constant among generations (postzygotic constraint).

3. Random mating

This section summarizes the outcomes for the case of random mating (no prezygotic restrictions). Although most of the results described here can be found in the literature (see for example [22]), they are important as a reference for the results presented in the next section.

If random mating is assumed, $w_{h_1:h_2} = w_{RM}$ for every encounter. Substituting in Eqs. (1)–(4) and summing up, we obtain

$$N^{t+1} = w_{RM}N^t(N^t-1)/2. \tag{9}$$

Imposing $N^{t+1} = N^t \equiv N$, for very large populations we obtain $w_{RM} = 2/N$. Introducing the linkage disequilibrium $D^t = p^t_{AB}p^t_{ab} - p^t_{Ab}p^t_{aB}$, the equations for the haplotype frequencies are greatly simplified and can be written as

$$p^{t+1}_{AB} = p^t_{AB} - rD^t \tag{10}$$
$$p^{t+1}_{Ab} = p^t_{Ab} + rD^t \tag{11}$$
$$p^{t+1}_{aB} = p^t_{aB} + rD^t \tag{12}$$
$$p^{t+1}_{ab} = p^t_{ab} - rD^t. \tag{13}$$

A sufficient condition for equilibrium is $D^t = 0$, or $p^t_{AB}p^t_{ab} = p^t_{Ab}p^t_{aB}$. Notice that the quantities

$$\tilde{p}^t_A = p^t_{AB} + p^t_{Ab} \tag{14}$$
$$\tilde{p}^t_a = p^t_{aB} + p^t_{ab} = 1 - \tilde{p}^t_A \tag{15}$$
$$\tilde{p}^t_B = p^t_{AB} + p^t_{aB} \tag{16}$$
$$\tilde{p}^t_b = p^t_{Ab} + p^t_{ab} = 1 - \tilde{p}^t_A, \tag{17}$$

representing the frequencies of the four alleles, remain constant from the first generation (we will therefore omit the superscript t from now on). This is also the case in the context of the Hardy–Weinberg (HW) equilibrium, however it should be emphasized that in the present framework there are two independent allele frequencies (because $\tilde{p}_A+\tilde{p}_a=\tilde{p}_B+\tilde{p}_b=1$) in contrast to the HW equilibrium where the only independent variable is the frequency of one of the two available alleles in a single-locus diploid genome.

From Eqs. (10)–(13) we obtain

$$D^{t+1}=(p^t_{AB}-rD^t)(p^t_{ab}-rD^t)-(p^t_{Ab}+rD^t)(p^t_{aB}+rD^t)=rD^t, \tag{18}$$

whose solution is simply

$$D^t=r^tD^0, \tag{19}$$

D^0 being the initial value of D. Combining (14)–(17) and (10)–(13), we obtain the following relationships

$$p^t_{AB}=\tilde{p}_A\tilde{p}_B+D^t=\tilde{p}_A\tilde{p}_B+r^tD^0 \tag{20}$$
$$p^t_{Ab}=\tilde{p}_A\tilde{p}_b-D^t=\tilde{p}_A\tilde{p}_b-r^tD^0 \tag{21}$$
$$p^t_{aB}=\tilde{p}_a\tilde{p}_B-D^t=\tilde{p}_a\tilde{p}_B-r^tD^0 \tag{22}$$
$$p^t_{ab}=\tilde{p}_a\tilde{p}_b+D^t=\tilde{p}_a\tilde{p}_b+r^tD^0. \tag{23}$$

Accordingly, the haplotype frequencies reach an equilibrium characterized by multiplicative combinations of the alleles frequencies involved,

$$p^{\mathrm{eq}}_{AB}=\tilde{p}_A\tilde{p}_B \tag{24}$$
$$p^{\mathrm{eq}}_{Ab}=\tilde{p}_A\tilde{p}_b \tag{25}$$
$$p^{\mathrm{eq}}_{aB}=\tilde{p}_a\tilde{p}_B \tag{26}$$
$$p^{\mathrm{eq}}_{ab}=\tilde{p}_a\tilde{p}_b. \tag{27}$$

Haplotype frequencies in this state are said to be in linkage equilibrium.

The conservation of the allele frequencies across generations can be seen as a physical conservation law with the practical importance of allowing the calculation of the equilibria directly from the initial conditions, i. e., without solving the dynamical equations.

The result (24)–(27) is similar to the HW theorem, in which the genotype frequencies are factorized in terms of the alleles frequencies at the maternal and paternal chromosomes. Linkage equilibrium, however, is only attained here asymptotically (Eqs. (20)–(23)), in contrast to the HW theory in which the equilibrium of the genotype frequencies is attained in a single generation.

4. Assortative mating

To mathematically describe the mating restrictions imposed on individuals differing in more than one locus, we define the rates $w_{h_1:h_2}$ as follows:

$$w_{h_1:h_2}=\begin{cases}0 & \text{for } h_1:h_2=AB:ab \text{ or } h_1:h_2=Ab:aB\\ w_{AM} & \text{otherwise.}\end{cases} \tag{28}$$

Replacing the previous definition in (1)–(4), and proceeding exactly as in Section 3, in the limit of very large populations we obtain

$$w_{AM}=w_{RM}\frac{1}{1-2\Delta^t}=\frac{2}{N}\left(\frac{1}{1-2\Delta^t}\right), \tag{29}$$

with

$$\Delta^t\equiv\frac{N^t_{AB}N^t_{ab}+N^t_{Ab}N^t_{aB}}{N^2}=p^t_{AB}p^t_{ab}+p^t_{Ab}p^t_{aB}. \tag{30}$$

Contrary to w_{RM}, w_{AM} is not constant but varies according to the number of encounters taking place. The larger the number of incompatible encounters the bigger the chance that a compatible encounter results in viable offspring.

Table 2
The four types of fixed points of the dynamical system (31)–(34). Fixed points of types 1 and 2 correspond to equilibrium solutions where one or two alleles are absent. These absent alleles label the fixed points. Point E_B, for instance, corresponds to a population with haplotypes *Ab* and *ab*, where three alleles and two haplotypes can be found. Therefore, indicating the allele that is lost, *B*, is easier than indicating all that is left.

Type	Label	Coordinates	Stability
Type 1. Continuous sets. Two compatible haplotypes have zero frequency; one allele is lost at one locus. The other locus remains polymorphic.	E_A	$p_{AB} = p_{Ab} = 0$, $p_{aB} = \lambda_A$, $p_{ab} = 1 - \lambda_A$	Stable
	E_B	$p_{AB} = p_{aB} = 0$, $p_{Ab} = \lambda_B$, $p_{ab} = 1 - \lambda_B$	
	E_a	$p_{aB} = p_{ab} = 0$, $p_{AB} = \lambda_a$, $p_{Ab} = 1 - \lambda_a$	
	E_b	$p_{Ab} = p_{ab} = 0$, $p_{AB} = \lambda_b$, $p_{aB} = 1 - \lambda_b$	
		$\lambda_{A,B,a,b} \in (0, 1)$	
Type 2. Three haplotypes have zero frequency. One allele is lost at both loci.	E_{AB}	$p_{AB} = p_{Ab} = p_{aB} = 0$, $p_{ab} = 1$	Stable
	E_{aB}	$p_{AB} = p_{aB} = p_{ab} = 0$, $p_{Ab} = 1$	
	E_{ab}	$p_{Ab} = p_{aB} = p_{ab} = 0$, $p_{AB} = 1$	
	E_{Ab}	$p_{AB} = p_{Ab} = p_{ab} = 0$, $p_{aB} = 1$	
Type 3. Two incompatible haplotypes have zero frequency.	EU_1	$p_{Ab} = p_{aB} = 0$, $p_{AB} = p_{ab} = 1/2$	Unstable
	EU_2	$p_{AB} = p_{ab} = 0$, $p_{Ab} = p_{aB} = 1/2$	
Type 4. Equiprobable distribution.	ES	$p_{AB} = p_{Ab} = p_{aB} = p_{ab} = 1/4$	Saddle

By substituting (29) in (28), and (28) in (1)–(4), equations for the haplotype frequencies reduce to

$$p_{AB}^{t+1} = \frac{p_{AB}^t(1 - p_{ab}^t)}{1 - 2\Delta^t} \tag{31}$$

$$p_{Ab}^{t+1} = \frac{p_{Ab}^t(1 - p_{aB}^t)}{1 - 2\Delta^t} \tag{32}$$

$$p_{aB}^{t+1} = \frac{p_{aB}^t(1 - p_{Ab}^t)}{1 - 2\Delta^t} \tag{33}$$

$$p_{ab}^{t+1} = \frac{p_{ab}^t(1 - p_{AB}^t)}{1 - 2\Delta^t}. \tag{34}$$

Two things must be pointed out concerning Eqs. (31)–(34). In the first place, it is now transparent the fact that assortative mating induces sexual selection. For instance, the factor $(1 - p_{ab})$ in Eq. (31) can be interpreted as the mean fitness of the haplotype *AB* (which is the proportion of compatible partners within the population), and the denominator as the mean fitness of the population. Secondly, as the terms involving the recombination rate correspond exactly to the incompatible encounters (see Table 1), these terms do not appear in Eqs. (31)–(34), making our assortative system independent of the selected recombination scheme.

In what follows, we explore the dynamics governed by Eqs. (31)–(34) on the basis of a fixed point stability analysis.

4.1. Equilibrium solutions and stability analysis

Eqs. (31)–(34) display four different types of fixed points, summarized in Table 2. As demonstrated next, only types 1 and 2 are stable.

Since $p_{AB} + p_{Ab} + p_{aB} + p_{ab} = 1$, it is possible to give a graphical description of the dynamics by constructing a three-dimensional phase space. We arbitrarily chose the frequencies p_{AB}, p_{Ab} and p_{aB} as the independent dynamic variables. The constraints $p_{AB} \geq 0$, $p_{Ab} \geq 0$, $p_{aB} \geq 0$, and $p_{AB} + p_{Ab} + p_{aB} \leq 1$ give the phase space the geometry of a tetrahedron having right triangular faces (Fig. 1). The top face of the tetrahedron, defined by the equation $p_{AB} + p_{Ab} + p_{aB} = 1$, corresponds to frequency distributions having $p_{ab} = 0$, whereas the origin of the coordinate system corresponds to $p_{ab} = 1$. Type 1 fixed points are located at four of the six edges of the tetrahedron (colored edges in Fig. 1), the points of type 2 are the vertices of the tetrahedron (black circles), type 3 fixed points EU_1 and EU_2 are located at the midpoints of the edges not containing points of type 1 (orange circles) and finally, the center of the tetrahedron houses the type 4 fixed point *ES* (brown circle).

We start the discussion with type 3 fixed points, for which the stability matrix is two times the identity. There is, therefore, a single fully degenerated eigenvalue $\zeta = 2$ indicating that both points EU_1 and EU_2 are unstable.

The stability matrix of *ES* displays two different eigenvalues, $\zeta_s = 2/3$ and $\zeta_u = 4/3$, the latter with degeneration 2. Accordingly, this fixed point has a saddle like behavior, being unstable on a two-dimensional subspace and stable on a one-dimensional subspace. From a geometrical point of view, it is interesting to note that the points EU_1 and EU_2 are co-linear and equidistant with respect to the point *ES*, and the line that houses the three points (from now on, the EU_1—ES—EU_2 axis) corresponds to the subspace spanned by the stable eigenvector $\mathbf{v}_s = \mathbf{e}_{AB} - \mathbf{e}_{Ab} - \mathbf{e}_{aB}$, where $\mathbf{e}_{AB}$, $\mathbf{e}_{Ab}$, and $\mathbf{e}_{aB}$ designate the unitary vectors in the corresponding directions.

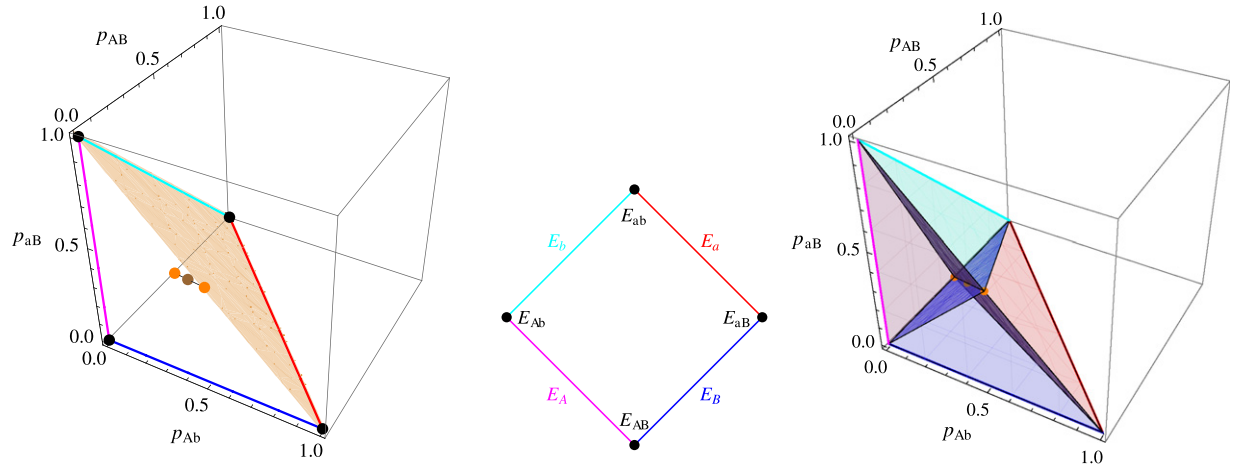

Fig. 1. Left: three-dimensional phase space displaying the four families of equilibrium solutions: E_A (p_{aB} axis, purple), E_B (p_{Ab} axis, blue), E_a (diagonal on the $p_{Ab} - p_{AB}$ plane, red) and E_b (diagonal on the $p_{aB} - p_{AB}$ plane, cyan); E_{ab}, E_{Ab}, E_{aB} and E_{AB} (vertices connecting the first family, black circles); EU_1 and EU_2 (midpoints of edges of the phase space not containing the first family, orange circles); and ES (center, brown circle). The shaded light brown surface represents the top face of the tetrahedral phase space of equation $p_{AB} + p_{Ab} + p_{aB} = 1$. Middle: schematic representation of the stable fixed points. Right: division of the phase space displaying the basins of attraction of type 1 fixed points. (For interpretation of the references to color in this figure legend, the reader is referred to the web version of this article.)

Fixed points of types 1 and 2 deserve a more detailed description. While not displaying exactly the same properties, they share common features, which make it instructive to analyze the stability of both types at the same time. We take as an example the set of points E_B, and its $\lambda_B \to 0$ and $\lambda_B \to 1$ limits, which are the points E_{AB} and E_{aB}, respectively. Appendix A explains how to transfer the outcomes of the following analysis to the remaining type 1 and type 2 fixed points. The stability matrix for any of such points has the following eigenvalues and eigenvectors:

- $\zeta_1 = \lambda_B$: $\mathbf{v}_1 = \frac{1}{2}\mathbf{e}_{AB} - \lambda_B \mathbf{e}_{Ab}$.
- $\zeta_2 = 1 - \lambda_B$: $\mathbf{v}_2 = (\frac{1}{2} - \lambda_B)\mathbf{e}_{Ab} + \frac{1}{2}\mathbf{e}_{aB}$.
- $\zeta_3 = 1$: $\mathbf{v}_3 = \mathbf{e}_{Ab}$.

The fixed points are degenerated along the direction spanned by $\mathbf{v}_3$. Indeed, an initial condition close to the fixed point, displaced along that direction, corresponds to a new point of the set E_B, i. e., to a new fixed point sharing the same behavior. As the dynamics is constrained to planes which do not contain that direction (see Section 4.3), those displacements cannot be achieved by the dynamics itself, so the overall stability is governed by the behavior of the system in the remaining two eigen-directions. This is consistent with the fact that $\zeta_3 = 1$ for any λ_B.

In the directions spanned by $\mathbf{v}_1$ and $\mathbf{v}_2$, the fixed points E_B are stable since the corresponding eigenvalues are smaller than one. The points E_{AB} and E_{aB} are also stable, however their stability cannot be inferred from the eigenvalues. The eigenvectors $\mathbf{v}_1$ and $\mathbf{v}_2$ have the interesting property of pointing from the fixed points E_B (as well as from E_{AB} and E_{aB}) to the points EU_1 and EU_2, respectively (see Fig. 2). The importance of this property will be evident in the Sections 4.3 and 5.

4.2. Rates of convergence

Although the fixed points E_{AB} and E_{aB} have the same qualitative behavior as the points in the set E_B (one degenerated direction and two stable directions pointing to type 3 fixed points), they differ in the time to convergence. Close to the fixed points the movement along a given eigendirection obeys

$$x_i^{t+1} = \zeta_i x_i^t, \tag{35}$$

so that

$$x_i^t = x_i^0 \zeta_i^t \equiv x_i^0 e^{-t/\tau_i}, \tag{36}$$

(x_i^0 being the ith component of the initial displacement from the fixed point, for $i = 1, 2$) with

$$\tau_i = -\frac{1}{\ln \zeta_i}. \tag{37}$$

The ratio between the time constants in the directions $\mathbf{v}_1$ and $\mathbf{v}_2$ is, therefore,

$$\frac{\tau_1}{\tau_2} = \frac{\ln(1 - \lambda_B)}{\ln \lambda_B}. \tag{38}$$

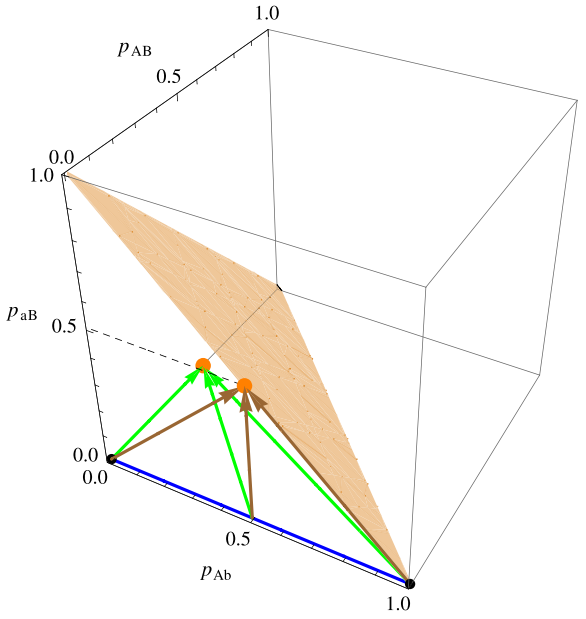

Fig. 2. Eigenvectors $\mathbf{v_1}$ (green) and $\mathbf{v_2}$ (brown) corresponding to the points E_B (with $\lambda_B = 1/2$), E_{AB} and E_{aB}. The blue line represents the entire set E_B which is parallel to the vectors $\mathbf{v_3}$ (not shown). (For interpretation of the references to color in this figure legend, the reader is referred to the web version of this article.)

Accordingly, for fixed points close to the point E_{AB} ($\lambda_B \sim 0$), the time to convergence along $\mathbf{v}_2$ is larger than the time along $\mathbf{v}_1$. The opposite behavior is obtained for fixed points close to E_{aB} ($\lambda_B \sim 1$).

For λ_B strictly equal to zero, the estimation (37) yields an infinitely slow convergence along $\mathbf{v}_2$, and an instantaneous convergence along $\mathbf{v}_1$. This is however a consequence of the attempt to linearize an equation with no linear contribution in its series expansion. Since $p_{Ab} = p_{aB} = 0$ along $\mathbf{v}_1$, we can rewrite Eq. (31) as

$$p_{AB}^{t+1} = \frac{(p_{AB}^t)^2}{1 - 2p_{AB}^t(1 - p_{AB}^t)}, \tag{39}$$

whose leading order is quadratic. We write therefore

$$p_{AB}^{t+1} = (p_{AB}^t)^2 + O((p_{AB}^t)^3) \tag{40}$$

for points close to E_{AB}, whose leading order solution reads

$$p_{AB}^t = (p_{AB}^0)^{2^t}. \tag{41}$$

Besides demonstrating stability, this solution shows that convergence is superfast in comparison to the exponential behavior for points E_B (Eq. (36)).

In the direction spanned by $\mathbf{v}_2$, $p_{Ab} = p_{aB}$ and $p_{AB} = 0$. Therefore, we rewrite Eq. (32) as

$$p_{Ab}^{t+1} = \frac{p_{Ab}^t(1 - p_{Ab}^t)}{1 - 2(p_{Ab}^t)^2} = p_{Ab}^t(1 - p_{Ab}^t) + O((p_{Ab}^t)^3). \tag{42}$$

Even by neglecting the term of $O(p_{Ab}^3)$, this equation does not have a closed solution.[1] Yet, it is possible to extract a conclusion concerning stability and convergence rate. Successive iterations of Eq. (42) give

$$p_{Ab}^t = p_{Ab}^0 \sum_{k=0}^{2^t-1} (-1)^k a_k (p_{Ab}^0)^k, \tag{43}$$

where $a_0 = 1$ and $a_1 = t$. Accordingly, for times $t < O(1/p_{Ab}^0)$ and points close to the fixed point along $\mathbf{v}_2$,

$$p_{Ab}^t \approx p_{Ab}^0(1 - tp_{Ab}^0) \approx \frac{p_{Ab}^0}{1 + p_{Ab}^0 t}, \tag{44}$$

[1] The equation is a particular case of the logistic map $x_{n+1} = rx_n(1 - x_n)$, having analytical solutions only for $r = -2$, $r = 2$ and $r = 4$.

which again demonstrates stability, however convergence proceeds superslowly when compared with points E_B. Numerical computations demonstrate that the right hand result is still valid for times arbitrarily large (see Appendix B).

4.3. Conserved quantities

Quantities not changing in time give powerful insights into dynamical problems. When individuals mate at random, allele frequencies (14)–(17) remain constant, and this property characterizes the equilibrium. Surprisingly, the dynamics under assortative mating reveals the existence of a new conserved quantity, which again allows for a complete characterization of the dynamics.

From Eqs. (31)–(34) it follows that all allele frequencies obey the same evolution equation

$$\tilde{p}_u^{t+1} = \frac{\tilde{p}_u^t - 1/2}{1 - 2\Delta^t} + 1/2, \tag{45}$$

with $u = A, B, a, b$. Writing Eq. (45) for $u = A$ and for $u = B$, and dividing one equation by the other, implies that the quantity

$$T = \frac{\tilde{p}_A^t - 1/2}{\tilde{p}_B^t - 1/2} \tag{46}$$

remains constant across generations. In turn, this implies that in the three-dimensional haplotype space the dynamics is constrained to a plane defined by the equation

$$p_{AB}^t + p_{Ab}^t - 1/2 - T(p_{AB}^t + p_{aB}^t - 1/2) = 0, \tag{47}$$

referred to, from now on, as a plane of motion. Notice that for any value of T, points in the $EU_1 - ES - EU_2$ axis satisfy the previous equation, implying that this axis is contained in all planes of motion. In fact, a change in the specific value of T signifies a rotation of the plane around the $EU_1 - ES - EU_2$ axis. The latter characteristic of the haplotype space immediately provides a way to describe the dynamics in a quite simple fashion. Specifically, the location of a plane of motion (obtained from initial conditions through (46) and (47)) unambiguously determines two stable fixed points, which can be

1. E_B and E_b for $|T| < 1$
2. E_A and E_a for $|T| > 1$
3. E_{AB} and E_{ab} for $T = 1$
4. E_{Ab} and E_{aB} for $T = -1$

Once the plane of motion is determined (in Fig. 3 we illustrate the situation for $T = -0.8$), and the two stable fixed points are preselected according to the previous relationships (in the example of Fig. 3 the preselected points are type 1 fixed points E_B and E_b), each of these fixed points gives rise to a pair of stable eigenvectors $\mathbf{v}_1$ and $\mathbf{v}_2$ that run along the borders of the plane of motion. Accordingly, the dynamics is reduced to a two-dimensional hyperbolic motion with the central fixed point ES attracting trajectories in one direction (corresponding to the $EU_1 - ES - EU_2$ axis) and repelling trajectories in the other direction. The latter, unstable direction, gives rise to the unstable manifold connecting ES with the two stable fixed points.

The only ambiguity remaining concerns which of the two stable fixed points intersected by the plane of motion will be attained. Of course, this ambiguity is solved by determining on which side of the $EU_1 - ES - EU_2$ axis the initial condition is located (see Fig. 3). As we demonstrate next, a simple recipe to determine the latter issue consists in computing the initial values of the allele frequencies (14)–(17), and identifying the allele in the smallest proportion.

The right panel of Fig. 1 depicts a division of the haplotype space in four regions, and two planes forming the frontiers separating the regions. These planes correspond to $T = 1$, and $T = -1$. In terms of the alleles frequencies, a straightforward calculation shows that on the former plane $\tilde{p}_A = \tilde{p}_B$, whereas on the latter plane $\tilde{p}_A + \tilde{p}_B = 1$. Accordingly, in one and only one of the four regions, the alleles frequencies should satisfy

- $\tilde{p}_A < \tilde{p}_B$
- $\tilde{p}_A + \tilde{p}_B < 1$

But the second relation implies $\tilde{p}_A < \tilde{p}_b$, which necessarily means $\tilde{p}_A < 1/2$ and thus $\tilde{p}_A < \tilde{p}_a$. This region of the haplotype space is therefore characterized by the fact that the allele A is the allele in the smallest proportion. As type 1 fixed points labeled E_A (in purple in Fig. 1) have necessarily this property, it turns out that the region in consideration must contain all points in the phase space that are attracted to this set of fixed points. The latter observations lead to the conclusion that the points shadowed in light purple in Fig. 1 have the allele A in the smallest proportion and evolve to fixed points E_A. An equivalent argumentation allows to conclude that the light blue region contains initial conditions having allele B in the smallest proportion (which evolve to fixed points E_B), light red region contains initial conditions with allele a in the smallest

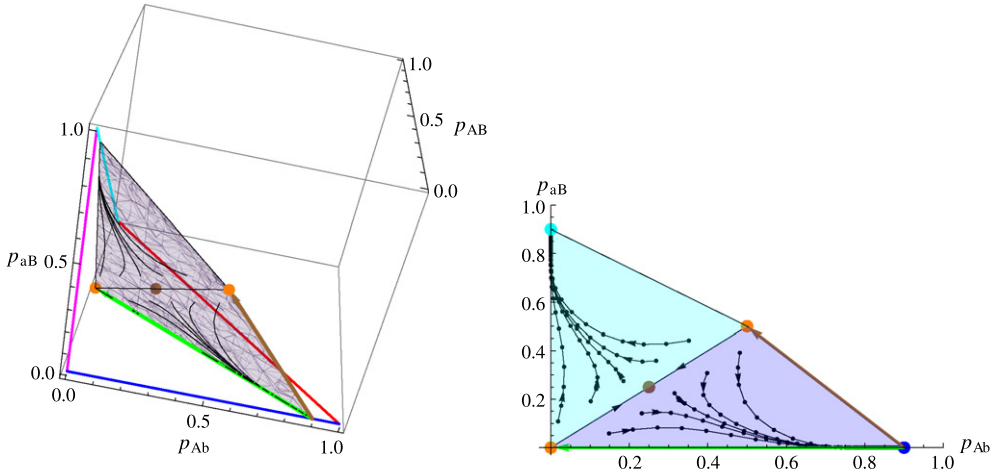

Fig. 3. Plane of motion corresponding to $T = -0.8$, and a set of trajectories with initial conditions chosen close to the stable manifold of the point *ES*. In the right panel, a projection of the plane of motion on the $p_{Ab} - p_{aB}$ plane. Arrows indicate the direction of motion, and shadowed regions represent the basins of attraction of the fixed points E_b (cyan) and E_B (blue) (in the left panel, these points are the intersections of the plane with the cyan and blue lines, containing the entire sets E_b and E_B, respectively). In green and brown, the eigenvectors of the equilibrium point E_B. Notice the bending of the trajectories toward $\mathbf{v_1}$ (green vector), making evident the differential rates of convergence in the two eigendirections. In the picture $\lambda_B = 0.9$, which corresponds to $\tau_1/\tau_2 \approx 21.8$. (For interpretation of the references to color in this figure legend, the reader is referred to the web version of this article.)

proportion (which evolve to fixed points E_a), and finally, light cyan region contains initial conditions with allele *b* in the smallest proportion (which evolve to fixed points E_b).

4.4. Equilibrium

The construction presented above allows to predict, for an arbitrary initial condition, the asymptotic equilibrium of the population in terms of two elements. First, it is necessary to establish the plane of motion where the initial condition is located (the value of the constant T), and second, among the four initial alleles it must be identified the allele in the smallest proportion. In the example of Fig. 3, a bunch of trajectories is simulated taking initial conditions close to the $EU_1 - ES - EU_2$ axis and having $T = -0.8$. The plane of motion intersects the set E_B for initial conditions having *B* in the smallest proportion and the set E_b for initial conditions having *b* in the smallest proportion. From the conservation of $T = -0.8$ results that at equilibrium the first bunch of trajectories converges to the point given by $\lambda_B = 0.9$, and the second bunch of trajectories to the point given by $\lambda_b = 0.1$.

From the analysis of the previous paragraph can be extracted a very practical result. First, the fact that among the four initial allele frequencies, the one in the smallest proportion always evolves to zero. This information, together with the knowledge of the conserved quantity T, suffices to determine all allele frequencies at equilibrium. For instance, if $\tilde{p}_b$ is the smallest initial frequency (in the example of Fig. 3 such an initial condition would be placed in the light cyan region of the haplotype space), at equilibrium $\tilde{p}_b = 0$ and therefore $\tilde{p}_B = 1$. From Eq. (46) results $\tilde{p}_A = (1 + T)/2$ and $p_a = 1 - p_A = (1 - T)/2$. Moreover, once the allele frequencies are determined as described above, the fact that stable equilibria have at least one fixed allele makes haplotype equilibrium solutions to behave as if they were single locus solutions. Therefore, haplotype frequencies are in linkage equilibrium as in random mating (Eqs. (24)–(27)). We stress that the latter property is not general but must be regarded as a consequence of this (and possibly others) mating system, and which will be of extreme utility when an arbitrary number of loci is taken into account.

5. Conclusions and biological implications

Together, the procedure outlined in Sections 4.3 and 4.4 to predict the equilibrium from the initial conditions, and the information provided in Section 4.2 concerning times to convergence, represent the solution of the dynamics of the two-loci problem subjected to assortative mating. Geometrically, the dynamics reduces to a foliation of the three-dimensional haplotype space in planes with a very simple motion, consisting of a central hyperbolic point repelling trajectories toward two stable equilibria. Initial conditions and stable equilibria remain related through the existence of a conserved quantity T, which defines the planes where the hyperbolic motion takes place.

On the basis of the times to convergence, and taking into account that convergence is governed by the slowest of the two stable directions $\mathbf{v}_1$ and $\mathbf{v}_2$, the stable equilibria can be divided in two categories. Stable equilibria of type 1 are attained exponentially (with a characteristic time given by $\max\{\tau_1, \tau_2\}$), whereas type 2 equilibria are attained at much slower rates ($\delta^t = \frac{\delta^0}{1+\delta^0 t}$, δ being the distance to the fixed point). It is interesting to observe that this classification has a biological

counterpart. Specifically, slow-attained equilibria represent monomorphic populations, whereas exponentially-attained equilibria correspond to populations that are polymorphic at a single locus. Double-polymorphic populations are represented by the unstable fixed points of types 3 and 4, or evolve to any of the former scenarios. Biologically, type 3 fixed points correspond to sympatric speciation, and the fact they are unstable shows that sympatry fails to happen in this framework, whereas the type 4 fixed point corresponds to the maximum disordered situation in which the four haplotypes have the same frequency. The latter configuration can be stabilized by introducing a sufficiently large mutation rate, as will be demonstrated in a future work.

An explanation for the differential speeds of convergence to the stable fixed points in the directions $\mathbf{v}_1$ and $\mathbf{v}_2$ can be as follows. Let us consider the type 2 fixed point E_{AB} for simplicity. Convergence along $\mathbf{v_1}$, i.e., along the axis p_{AB} in the 3-dimensional haplotype space (see Fig. 2), means that there is a competition between haplotypes *AB* and *ab*. The closer the population gets to the equilibrium, that is, the rarer the haplotype *AB* becomes, the stronger the sexual selection is against this type (because the probability of finding a compatible mating partner decreases). Individuals with the abundant haplotype *ab*, instead, succeed almost always in finding a compatible pair *ab*, leading to a fast convergence to the monomorphic population *ab*, i.e., to the fixed point E_{AB}. In contrast, convergence along $\mathbf{v_2}$ means that there is competition between the haplotype *ab* on the one hand, and the incompatible pair $aB - Ab$ on the other hand. Individuals with the haplotype *ab* can mate with any other member of the population, whereas individuals with haplotypes *aB* and *Ab* lose some reproductive opportunities due to failed mating attempts with an incompatible haplotype. As encounters between *ab* and *Ab* or between *ab* and *aB* are likely to produce the rare alleles *Ab* and *aB*, this type of sexual selection decreases in strength and nearly vanishes as the equilibrium is approached, making the convergence to become slow.

As pointed out in [9], models of incompatibility based on genetic distance have two alternative interpretations. One interpretation corresponds to sexual haploid populations with fitness assigned to pairs of individuals (here fitness is included in the compatibility–viability selection rate $w_{h_1:h_2}$), and the second interpretation concerns diploid populations reproducing through random mating, where fitness is a function of individual heterozygosity. The model studied in this article describes thus an evolutionary process that eliminates double polymorphism (first interpretation), or alternatively a selection against double heterozygotes (second interpretation). Selection against heterozygotes, also known as underdominance, leads to disruptive selection which is one of the ingredients required for sympatric speciation. However, in addition to disruptive selection, sympatric speciation requires mechanisms that promote maintenance of polymorphism (e.g., advantage of rare types) [8,23]. Disruptive selection, as generated by assortative mating by itself, leads to positively frequency-dependent selection which destroys polymorphism and prevents speciation [2]. This is why sympatric speciation does not occur within the assortative mating framework discussed in this work.

Section 4.3 reveals another important aspect of assortativeness mediated by genetic distance, which concerns the fact that the allele initially appearing in the smallest proportion remains always in the smallest proportion, and vanishes when the equilibrium is attained. The existence of the conserved quantity T, in turn, also has an interesting consequence from the biological point of view. As $\tilde{p}_A = 1/2$ represents the maximum polymorphism at the first locus, $m_A = (\tilde{p}_A - 1/2)^2$ can be interpreted as a measure of the monomorphism for that gene. Therefore, the fact that $T^2 = m_A/m_B$ remains constant across evolution means an invariance in the relation between the monomorphisms, and thus between the polymorphisms, at the two loci. Namely, whenever a locus experiments a shift in its polymorphisms, this shift is carried to the polymorphism of the other locus.

In the general situation of B genes and a mating restriction by a genetic distance G, stable equilibria are expected to be of $G+1$ different types, in the form of fully monomorphic populations, polymorphic populations at a single locus, polymorphic populations at only two loci, up to polymorphic populations at the G loci. Accordingly, such scenarios can be related to an elimination of populations polymorphic at $G + 1$ to B loci, or alternatively to a selection against $G+1$ times to B times heterozygotes. These results will be demonstrated in a subsequent work.

In spatially structured populations individuals mate only with close neighbors, decreasing the mixing of alleles and slowing down the tendency to equilibrium. Locally, the dynamics of assortative mating drives the population to an equilibrium that depends on the (local) initial conditions, and it might happen that different regions converge to different equilibria, resulting in reproductively isolated species, similar to the simulations presented in [13]. As the case studied here exhibits reproductive isolation only in the trivial way accomplished by monomorphic species (for instance, populations *AB* and *ab* are isolated with a within-population genetic diversity $d_w = 0$), it is of special interest to explicitly consider the case $B = 3$ and $G = 1$. In this situation, populations $ABC - ABc$ and $abC - abc$ are reproductively isolated with $0 < d_w < 1$. Moreover, the existence of a third single polymorphic species $ABc - Abc$, or even the monomorphic species *Abc*, may create a ring structure, revealing the richness of scenarios that can be realized through this simple arrangement.

The simulations presented in [13] considered initial populations consisting of genetically identical individuals with variation introduced via mutations. However, since mutations are random and mating is local, allele correlation decreases with distance, leading to different distributions of alleles in different parts of space after a few generations. Once the number of accumulated mutations becomes of the order of G, assortative mating starts acting and (if the mutation rate is low) the results derived here should apply, leading to local populations that are polymorphic at approximately G loci and possibly reproductively isolated.

From the analysis of the times to convergence of Section 4.2, it is also expected that times to convergence for $G = 1$ behave in the same way even for $B > 2$, displaying an exponential behavior for single polymorphic species, and a superslow convergence for monomorphic species. The case $B = 3$ and $G = 2$, on the other hand, is expected to display three different

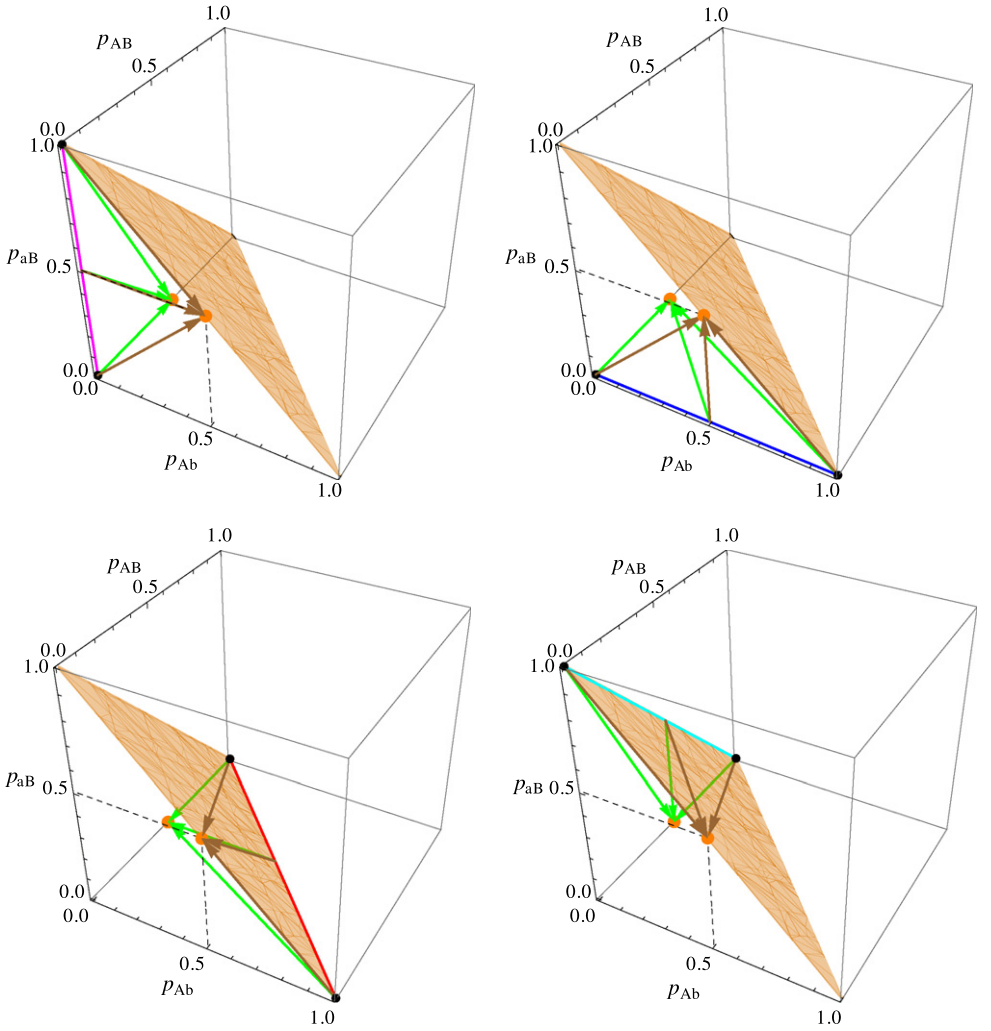

Fig. A.4. Eigenvectors corresponding to type 1 and type 2 fixed points (vectors $\mathbf{v}_1$ in green, and $\mathbf{v}_2$ in brown). (For interpretation of the references to color in this figure legend, the reader is referred to the web version of this article.)

temporal scales of convergence, corresponding to three types of stable equilibria. For finite populations these times to convergence should be compared with the time to fixation by random drift, which depends on the effective population size. The effects of drift and mutations will be the subject of a future publication.

Acknowledgments

We thank Yaneer Bar-Yam, Fernando Rossine and Paula Lemos for helpful discussions. We also thank the reviewers for their valuable comments and suggestions. This work was partly supported by FAPESP (Fundação de Amparo à Pesquisa do Estado de São Paulo) (grant no. 2009/11032-5) and CNPq (Conselho Nacional de Desenvolvimento Científico e Tecnológico) (grant no. 302858/2011-0).

Appendix A. Stability of fixed points of type 1 and 2 (complement)

In this appendix we extend the results of the stability analysis of Section 4.1 for the fixed points E_A, E_B and E_b. We start with the eigenvalues and eigenvectors of the stability matrices of the different fixed points.

Stability of points E_A (**purple line**, $p_{aB} = \lambda_A$)

- $\zeta_1 = \lambda_A$: $\mathbf{v}_1 = \frac{1}{2}\mathbf{e}_{Ab} - \lambda_A \mathbf{e}_{aB}$
- $\zeta_2 = 1 - \lambda_A$: $\mathbf{v}_2 = \frac{1}{2}\mathbf{e}_{Ab} + (\frac{1}{2} - \lambda_a)\mathbf{e}_{aB}$.
- $\zeta_3 = 1$: $\mathbf{v}_3 = \mathbf{e}_{aB}$.

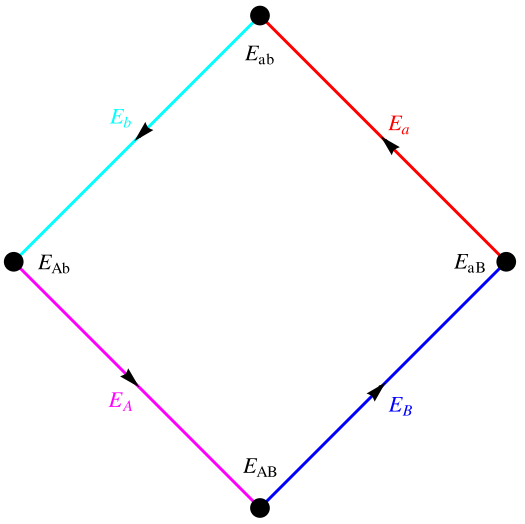

Fig. A.5. Schematic representation of type 1 and type 2 fixed points. Arrows indicate the direction of the walk employed in the text to describe the behavior of the rates of convergence. (For interpretation of the references to color in this figure legend, the reader is referred to the web version of this article.)

Stability of points E_a (**red line**, $p_{AB} = \lambda_a$, $p_{Ab} = 1 - \lambda_a$)

- $\zeta_1 = 1 - \lambda_a$: $\mathbf{v}_1 = (\frac{1}{2} - \lambda_a)\mathbf{e}_{AB} + (-1 + \lambda_a)\mathbf{e}_{Ab}$.
- $\zeta_2 = \lambda_a$: $\mathbf{v}_2 = -\lambda_a\mathbf{e}_{AB} + (-\frac{1}{2} + \lambda_a)\mathbf{e}_{Ab} + \mathbf{e}_{aB}$
- $\zeta_3 = 1$: $\mathbf{v}_3 = \mathbf{e}_{AB} - \mathbf{e}_{Ab}$.

Stability of points E_b (**cyan line**, $p_{AB} = \lambda_b$, $p_{aB} = 1 - \lambda_b$)

- $\zeta_1 = 1 - \lambda_b$: $\mathbf{v}_1 = (\frac{1}{2} - \lambda_b)\mathbf{e}_{AB} - (1 - \lambda_b)\mathbf{e}_{aB}$.
- $\zeta_2 = \lambda_b$: $\mathbf{v}_2 = -\lambda_b\mathbf{e}_{AB} + \mathbf{e}_{Ab} + (-\frac{1}{2} + \lambda_b)\mathbf{e}_{aB}$
- $\zeta_3 = 1$: $\mathbf{v}_3 = -\mathbf{e}_{AB} + \mathbf{e}_{aB}$.

Stable eigenvectors corresponding to points of type 1 and type 2, properly scaled, connect the fixed points with type 3 fixed points. In Fig. A.4 we expose this important property for some specific points at each set, including the points E_B analyzed in Section 4.1.

Rates of convergence are inferred from the relation

$$\tau_i = -\frac{1}{\ln \zeta_i} \tag{A.1}$$

where $i = 1, 2$ denotes the type 3 fixed point (EU_1 or EU_2) to which the eigenvector points. Accordingly, going through the set E_a from E_{aB} to E_{ab} (see Fig. A.5), makes τ_1 to decrease. This time becomes almost zero at the point E_{ab} (superfast convergence), and it starts increasing again by going to E_{Ab} through the set E_b (cyan line in Fig. A.5). At this τ_1 becomes infinite (superslow convergence), which means an equivalent behavior to that corresponding to E_{Ab}. On the other hand, as $\zeta_2 = 1 - \zeta_1$, it turns out that τ_2, the time to convergence along the directions spanned by $\mathbf{v}_2$, displays the opposite behavior. Finally, the picture is completed by observing that the remaining branch of the cycle ($E_{Ab} \to E_{AB}$ along E_A and $E_{AB} \to E_{aB}$ along E_B) is an exact repetition of the branch described above.

Appendix B. Numerical solution of Eq. (42)

Here we give a brief summary of the fitting process employed to solve Eq. (42). By iterating the map for different initial conditions and fitting the results, we obtain

$$p^t_{Ab} = \frac{1}{A(p^0_{Ab}) + t}, \tag{B.1}$$

where $A(x)$ is a function that diverges as $1/x$ when $x \to 0$ (see Fig. B.6). Accordingly, for very small p^0_{Ab} values we can write

$$p^t_{Ab} = \frac{p^0_{Ab}}{1 + p^0_{Ab}t} + O((p^0_{Ab})^2). \tag{B.2}$$

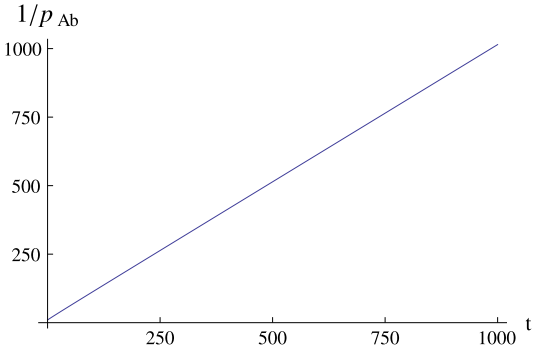

(a) Iterations of the map for the initial condition $p^0_{Ab} = 0.1$. The fitting gives $1/p_{Ab} = 12.336 + 1.002t$.

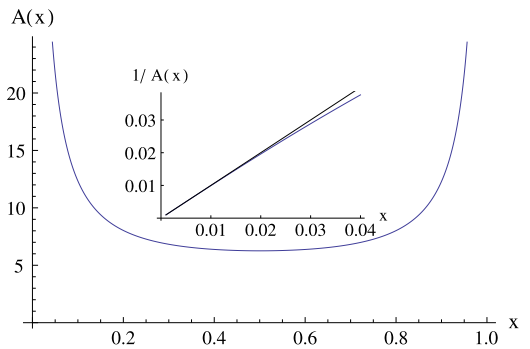

(b) Plot of the function A(x) (see the text). In the inset we plot $1/A(x)$ to demonstrate that, for very small x values $1/A(x) = x + 0(x^2)$ (black curve: $f(x) = x$).

Fig. B.6. Fitting results related to the eigenvector $\mathbf{v}_2$ of the stability matrix associated to E_{AB}. (For interpretation of the references to color in this figure legend, the reader is referred to the web version of this article.)

References

[1] J.A Coyne, H.A. Orr, Speciation, first ed., Sinauer Associates, Inc., 2004.
[2] S. Gavrilets, Fitness Landscapes and the Origin of Species (MPB-41), Princeton University Press, 2004.
[3] R.A. Butlin, et al., Trends Ecol. Evol. 27 (2012) 27.
[4] P. Nosil, Ecological Speciation, Oxford University Press, Oxford; New York, 2012.
[5] P.G. Higgs, B. Derrida, J. Phys. A. 24 (1991) L985.
[6] P.G. Higgs, B. Derrida, J. Mol. Evol. 35 (1992) 454.
[7] A.S. Kondrashov, M. Shpak, Proc. Soc. Lond R 265 (1998) 2273.
[8] U. Dieckmann, M. Doebeli, Nature 400 (1999) 354.
[9] S. Gavrilets, Am. Nat. 154 (1999) 1.
[10] G.A. Hoelzer, R. Drewes, J. Meier, R. Doursat, PLoS Comput. Biol. 4 (2008) e1000126.
[11] G.S.v. Doorn, P. Edelaar, F.J. Weissing, Science 326 (2009) 1704.
[12] B.M. Fitzpatrick, J.A. Fordyce, S. Gavrilets, J. Evol. Biol. 22 (2009) 2342.
[13] M.A.M. de Aguiar, M. Baranger, E.M. Baptestini, L. Kaufman, Y. Bar-Yam, Nature 460 (2009) 384.
[14] D. Ashlock, E.L. Clare, T.E. von Konigslow, W. Ashlock, J. Theoret. Biol. 264 (2010) 1202.
[15] M. Kopp, BioEssays 32 (2010) 564.
[16] C.J. Melian, C. Vilas, F. Baldo, E. Gonzalez-Ortegon, P. Drake, R.J. Williams, Ad. Ecol. Res. 45 (2011) 225.
[17] P. Desjardins-Proulx, D. Gravel, Am. Nat. 179 (2012) 137.
[18] S. Wright, Isolation by distance, Genetics. 28 (1943) 114.
[19] U. Candolin, Biol. Rev. 78 (2003) 575.
[20] J. Mallet, A. Meyer, P. Nosil, J.L. Feder, J. Evol. Biol. 22 (2009) 2332.
[21] K. Rose, E. Gurewitz, C. Fox, Phys. Rev. Lett. 65 (1990) 945.
[22] K.E. Holsinger, Lecture Notes in Population Genetics. http://darwin.eeb.uconn.edu/eeb348/lecture-notes/book.pdf.
[23] U. Dieckmann, M. Doebeli, J.A.J. Metz, D. Tautz, Adaptive Speciation, Cambridge University Press, Cambridge, 2012.